catalysts

MDPI

Article

Green and High Effective Scale Inhibitor Based on Ring-Opening Graft Modification of Polyaspartic Acid

Yongsheng Zhou [1], Jie Wang [2] and Yan Fang [2,*]

[1] School of Mechanical Engineering, Hefei University of Technology, Tunxi Road, Hefei 230009, China; zhouys19720708@126.com

[2] State Key Laboratory of Materials-Oriented Chemical Engineering, College of Biotechnology and Pharmaceutical Engineering, Nanjing Tech University, Nanjing 211816, China; wangj756722602@163.com

* Correspondence: fangyan@njtech.edu.cn; Tel.: +86-58139906

Abstract: Polyaspartic acid (PASP)-based green scale inhibitor has great potential application in water treatment. Here, we first synthesized PASP in ionic liquid. Then, an effective PASP-based green scale inhibitor was synthesized by ring-opening graft modification of PASP with both aspartic acid (ASP) and monoethanolamine (MEA). Its chemical composition was characterized by gel chromatography (GPC), Fourier transform infrared spectroscopy (FTIR), and 1H nuclear magnetic resonance (^{1}H NMR). Scale inhibition efficiency was measured by static scale inhibition tests. The results showed that the new PASP-based scale inhibitor has high scale inhibition to both $CaCO_3$ and $Ca_3(PO_4)_2$. When the concentration was increased to 2 mg/L, the inhibition efficiency of the new PASP-based scale inhibitor was 99% for $CaCO_3$, while when the concentration was raised to only 4 mg/L, its inhibition efficiency increased to 100% for $Ca_3(PO_4)_2$. Scanning electronic microscopy (SEM) and X-ray diffraction (XRD) were used to analyze the changes of crystal structure for $CaCO_3$ and $Ca_3(PO_4)_2$ after adding the new PASP-based scale inhibitor. The crystal size of $CaCO_3$ and $Ca_3(PO_4)_2$ became smaller and the crystal form became amorphous after adding the modified PASPs compared with adding pure PASP. Moreover, the modified PASP showed good biodegradation performance.

Keywords: polyaspartic acid; green synthesis; ring-openning graft modification; scaling inhibitor; biodegradation

Citation: Zhou, Y.; Wang, J.; Fang, Y. Green and High Effective Scale Inhibitor Based on Ring-Opening Graft Modification of Polyaspartic Acid. *Catalysts* **2021**, *11*, 802. https://doi.org/10.3390/catal11070802

Academic Editors: Jose M. Guisan and Gloria Fernandez-Lorente

Received: 23 February 2021
Accepted: 28 June 2021
Published: 30 June 2021

1. Introduction

In recent years, with the increase of worldwide population and expansion of modern society, the consumption and pollution of industrial water increases shortage of water resources significantly [1–3]. Water treatment is an important technology to deal with the shortage of water resources [4–6]. Among various methods explored for water treatment, the circulating cooling water system is widely utilized in industrial processes [7,8]. However, scale deposition is one of the major problems in this system [9]. Scales degrade the performance of heat exchangers by increasing the resistance to heat transfer and eventually result in tremendous economic loss due to energy waste by increasing the power requirements of pumps. In order to control scale formation, a variety of scale inhibitors have been explored and used widely in cooling water systems. Scale inhibitors are usually non-polymeric phosphonates (ATMP, HEDP, PBTC) and polymers with functional groups. The most common polymers are phosphonate, carboxylate, and sulfonate polymers. However, phosphonate and sulfonate polymers are being restricted due to environmental legislation [10–12]. With the increase of environmental awareness, environmentally friendly scale inhibitors have been drawing broad attention all over the world [13–17].

Polyaspartic acid (PASP) is a promising environmentally friendly scale inhibitor with nontoxicity and good biodegradability. It has excellent scale inhibiting performance for $CaCO_3$. However, its scale inhibiting performance for $Ca_3(PO_4)_2$ is poor. In order to improve the comprehensive scale inhibition performance of PASP, it is essential to modify

it by introducing functional groups into its side chain, such as hydroxyl groups, carboxylic groups, sulfonic groups, and/or phosphonyl groups [18,19].

Many studies have already reported on PASP modification. For example, Zhang et al. synthesized PASP/Urea by introducing an acylamino group into the side chains of PASP. It was shown that the modified PASP has better scaling inhibition to $CaSO_4$ [20]. Chen et al. synthesized Ser-PASP via introducing a hydroxylic group into the side chain of PASP. When Ser-PASP was added, the scale crystals became irregular, and complete inhibition to $CaSO_4$ was achieved [21]. Xu et al. obtained PASP–melamine grafted copolymer via polysuccinimide (PSI) ring-opening by melamine [22]. Xu et al. synthesized PASP/aminobenzenesulfonic acid (ABSA) copolymer using sulphanilic acid and PSI. It was found that the PASP/ABSA copolymer is able to efficiently inhibit $CaCO_3$ [23]. Although single-functional-group-modified PASP has shown improved scale inhibition to $CaCO_3$ and $CaSO_4$, it is still a challenge to achieve high scale inhibition to $Ca_3(PO_4)_2$.

Here, we prepared a new green and highly effective PASP-based scale inhibitor for water treatment (Figure 1). PASP was first synthesized in ionic liquid. Ionic liquids are a subset of molten salts with melting points at or below 100 °C [24]. Spurred by the green chemistry movement, ionic liquids are considered as promising alternative solvents to replace traditional volatile organic compounds (VOCs) due to their low volatility [25]. Then, a ring-opening graft modification strategy was adopted to modify the synthesized PASP with both aspartic acid (ASP) and monoethanolamine (MEA). The ASP and MEA provide a carboxyl and hydroxyl group to PASP, respectively. The introduced carboxyl can enhance the calcium chelation ability and solubilization for the crystals of $CaCO_3$ and $Ca_3(PO_4)_2$, while the hydroxyl group may result in distorting crystal lattices. In general, the synergy effect of the double-functional-group-modified PASP showed high scale inhibition performance for $CaCO_3$ and $Ca_3(PO_4)_2$, and it also showed good biodegradation performance.

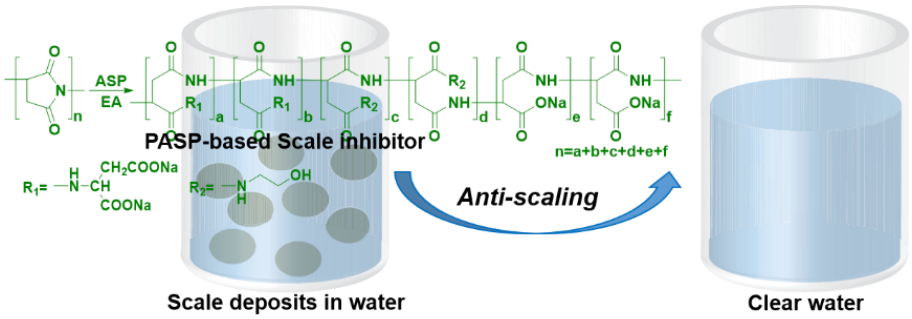

Figure 1. Schematic illustration of the new scale inhibitor based on ring-opening graft modification of polyaspartic acid for water treatment.

2. Results and Discussion

2.1. Ring-Opening Graft Modification of PASP

We first synthesized PASP in ionic liquid. Ionic liquid has unique advantages, including good thermal stability, strong solubility, nonvolatility, free design of anion and anion, etc. It can replace traditional organic solvents and catalysts to achieve green synthesis of PASP [26]. Then, a ring-opening graft modification strategy was adopted to modify PASP with both carboxyl and hydroxyl groups. Here, we put emphasis on discussing the graft modification process on the grafting ratio of ASP and MEA. The grafting ratio of both molecules are largely determined by the molar ratio of reagent (PSI–ASP–MEA), reaction time, and reaction temperature (Figure 2). First, the grafting ratio showed a significant increase with the increase of molar ratio of ASP and MEA (Figure 2a). When the molar ratio of the reagent (PSI–ASP–MEA) was fixed at 1:1:0, the grafting ratio of ASP was 74.0%, while when the molar ratio of the reagent (PSI–ASP–MEA) was fixed at 1:0:1, the grafting ratio of MEA was 89.8%. The difference of the grafting ratio for the two molecules may be ascribed to the difference of the steric hindrance effect between them. When successively increasing

the molar ratio of ASP or MEA, the grafting ratio of ASP and MEA obviously increased. This can be ascribed to the increased reaction probability during the whole reaction process. Typically, when the molar ratio of the reagent (PSI–ASP–MEA) was fixed at 1:0.5:0.5, the grafting ratio of ASP and MEA was probably 36.22% and 43.3%, respectively. Then, when increasing the reaction time from 12 h to 24 h, the increase first brought a significant enhancement of the grafting ratio for ASP from 32.8% to 36.2% and for MEA from 39.8% to 43.4%. This may be because there were more reactive sites generated during the initial reaction from 12 h to 24 h (Figure 2b). However, little change to the grafting ratios of either ASP or MEA occurred when further increasing the reaction time from 24 h to 60 h (Figure 2b). This indicates that the reaction reached equilibrium at 24 h. As shown in Figure 2c, the grafting ratio of both ASP and MEA decreased significantly when increasing the reaction temperature from 0 °C to 40 °C. Specifically, the grafting ratio of ASP decreased from 38.8% to 31.9%, and the grafting ratio of MEA decreased from 43.2% to 24.2%. As is well known, higher temperature usually leads to an increased number of active molecules, increased effective collision, and higher reaction rate. It should theoretically lead to an increased grafting ratio of both ASP and MEA during the fixed time. However, because the ring-opening graft modification is an exothermic reaction, the increased temperature inhibited the reaction process [27] and led to hydrolysis of the formed graft bond. Thus, the grafting ratio of both ASP and MEA inevitably decreased.

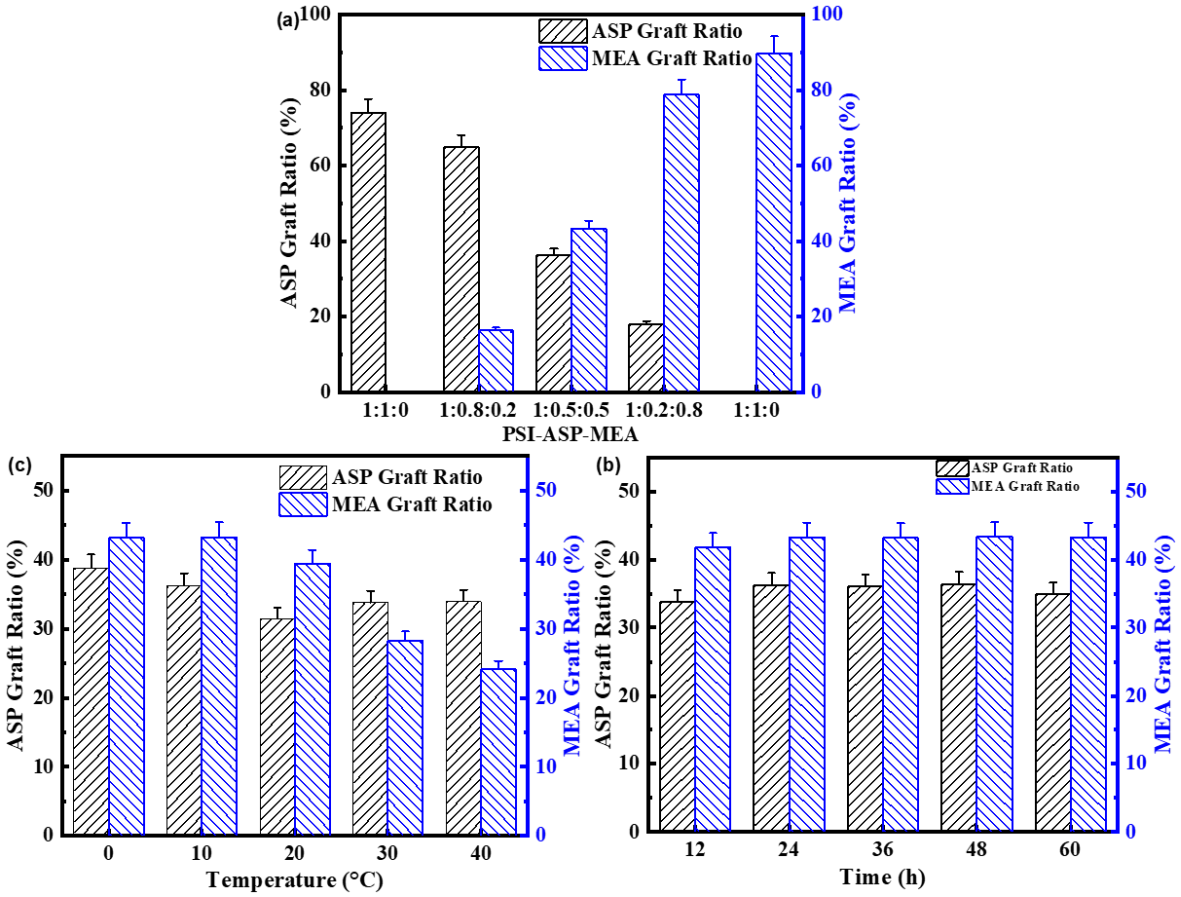

Figure 2. There are three typical influencing factors which affect graft ratio of ASP and MEA. (**a**) Influence of molar ratio of PSI–ASP–MEA on the graft ratio of ASP and MEA (reaction time is 24 h, reaction temperature is 0 °C); (**b**) influence of reaction time on the graft ratio of ASP and MEA (molar ratio of PSI–ASP–MEA is 1:0.5:0.5, reaction temperature is 0 °C); (**c**) influence of reaction temperature on the graft ratio of ASP and MEA (molar ratio of PSI–ASP–MEA was 1:0.5:0.5 and reaction time was 24 h).

2.2. Chemical Characterization of the Modified PASP

From Table 1, we can obtain the conclusion that the molecular mass of PASP synthesized in the ionic liquid was M_n 4.87 kDa (PDI~1.63). Compared with the pure PASP, GPC results show that the molecular mass of the modified PASP increased with the increase of MEA or ASP proportion in the monomer solution. Particularly, when the molar ratio of PSI–ASP–MEA was 1:0.5:0.5 (at reaction temperature of 0 °C and reaction time of 24 h), the molecular mass of the modified PASP was increased to M_n 4.90 kDa. The corresponding grafting ratios of ASP and MEA were calculated to be increased to 36.2% and 43.3%, respectively. This is reasonable, because increasing the molar ratio of ASP or MEA increases the grating ratio of the two molecules, inevitably enhancing the ring-opening graft modification. Thus, graft modification obviously increased the molecular weight of PASP.

Table 1. Molecular mass of PASP and the modified PASP calculated by GPC.

PSI-ASP-MEA	M_n (kDa)	M_w (kDa)	M_w/M_n
1:0:0	4.87	7.93	1.63
1:1:0	4.96	8.09	1.63
1:0.8:0.2	4.94	8.19	1.66
1:0.5:0.5	4.90	7.89	1.61
1:0.2:0.8	4.91	7.80	1.59
1:0:1	4.92	7.92	1.61

We then verified that the ASP and MEA were conjugated onto the PASP side chain by analyzing the molecular structure using FTIR (Figure 3). The absorption peaks at ~3422 cm^{-1}, ~1598 cm^{-1} and ~1401 cm^{-1} are attributed to the stretching vibration of N-H and C=O in –CONH and the absorption peak at C-N [28,29]. This indicates that the PASP was successfully synthesized in the ionic liquid. In addition, for the modified PASP, a peak corresponding to the stretching vibration of the C=O group was observed at ~1703 cm^{-1}, which indicates that the ASP was successfully grafted onto the side chain of PASP. Moreover, the stretching vibrations peak of the -C-O- group at ~1164 cm^{-1} and ~1064 cm^{-1} indicate that the MEA was successfully introduced to the side chain of PASP. In addition, 1H NMR was also used to verify the graft modification process (Figure S1). Proton NMR results show that for the PASP main chain, the peaks corresponding to -CH- and -CH_2- were observed at 4.45 ppm and 2.74 ppm, respectively. The peaks at 3.60~3.66 ppm and 3.16 ppm are attributed to -CH- and -CH_2- of the side chain for carboxyl group-modified PASP (PASP-ASP). Similarly, the peaks at 3.8 ppm and 3.12 ppm are attributed to -CH- and -CH_2- of the side chain for hydroxyl group-modified PASP (PASP-MEA). Furthermore, we obtained all of the above characteristic peaks for the product after both the carboxyl and hydroxyl group modifications to PASP, which indicates that the PASP-ASP-MEA was successfully synthesized.

2.3. Scale Inhibition Performance of the Modified PASP

To investigate the scale inhibition properties of the modified PASP, we chose $CaCO_3$ and $Ca_3(PO_4)_2$ as the two typical crystals. Figure 4a,b presents the scale inhibition performance of PASP-ASP-MEA against $CaCO_3$ and $Ca_3(PO_4)_2$ scales. When its concentration was 1 mg/L and 2 mg/mL, the inhibition efficiency of PASP-ASP-MEA against $CaCO_3$ scale reached 95% and 99%, respectively, while its inhibition efficiency against $Ca_3(PO_4)_2$ scale reached 75% and 89%, respectively. The maximum inhibition efficiency (100%) to both $CaCO_3$ and $Ca_3(PO_4)_2$ was achieved at a scale inhibitor dosage of 4 mg/L. Compared to PASP, PASP-ASP, and PASP-MEA, PASP-ASP-MEA had better inhibition performance against $CaCO_3$ and $Ca_3(PO_4)_2$ scales. The reasons may be listed as follows. Firstly, the sparingly soluble salts, such as $CaCO_3$, $Ca_3(PO_4)_2$, and gypsum, are crystallized on the nano/microdust impurities in the aqueous solution [30]. Those nano/microdusts are not uniform and consist of different ingredients. The antiscalants PASP and their derivatives

can block the nano/microdust crystallization centers of the salts. Therefore, the rate of crystallization of sparingly soluble salts decreases. Secondly, the grafted polymer has a better sorption on nano/microdust surface than a non-grafted one [31]. Because the nano/microdusts are not uniform, it is reasonable that some fractions of the dusts are better blocked by PASP-ASP and others by PASP-MEA. Thus, synergy becomes inevitable due to PASP-ASP-MEA combining the properties of PASP-ASP and PASP-MEA.

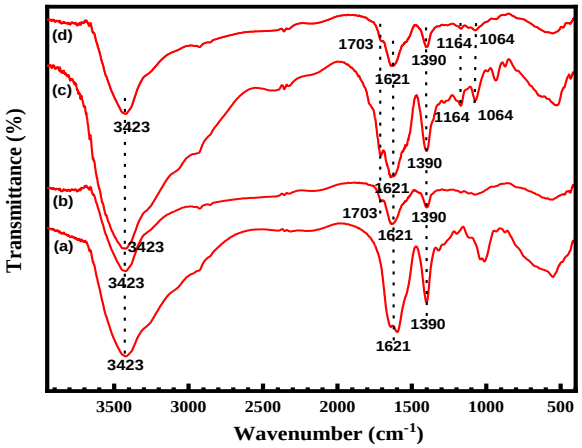

Figure 3. FTIR spectrum of PASP and PASP derivatives: (a) PASP, (b) PASP-ASP, (c) PASP-MEA, and (d) PASP-ASP-MEA. (For PASP-ASP-MEA, the molar ratio of PSI–ASP–MEA was 1:0.5:0.5, reaction temperature was 0 °C, and reaction time was 24 h).

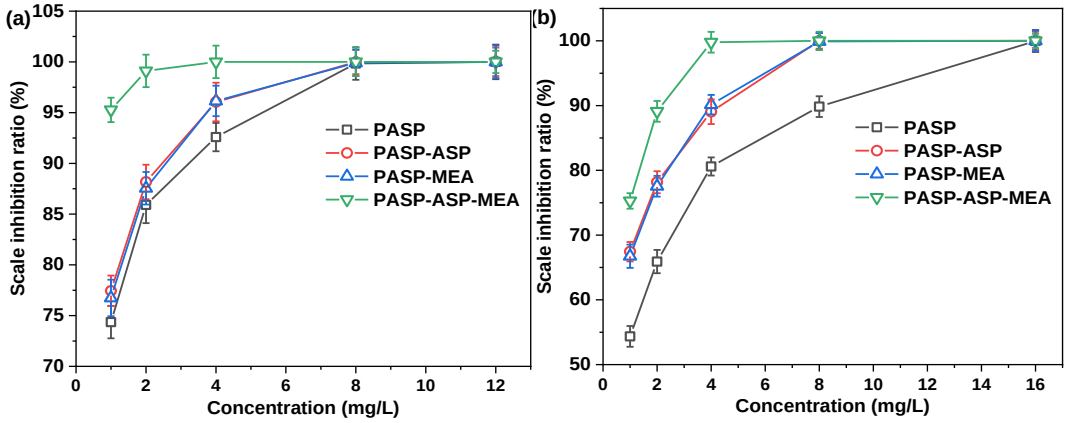

Figure 4. The inhibition efficiency of PASP and the modified PASPs (PASP-ASP, PASP-MEA, and PASP-ASP-MEA) against $CaCO_3$ scales (**a**) and $Ca_3(PO_4)_2$ scales (**b**). (For PASP-ASP-MEA, the molar ratio of PSI–ASP–MEA was 1:0.5:0.5, reaction temperature was 0 °C, and reaction time was 24 h).

The $CaCO_3$ and $Ca_3(PO_4)_2$ scale deposits were observed by scanning electron microscope (SEM). As shown in Figures 5 and 6, in the absence of PASP and the modified PASPs, $CaCO_3$ scale deposits show a calcite structure with regular shape and glossy surface, and $Ca_3(PO_4)_2$ scale deposits have an irregular polygon-shaped structure, not parallel to the surface to bulk. In comparison, when PASP and the modified PASPs were introduced into the solution, the shapes of $CaCO_3$ and $Ca_3(PO_4)_2$ scale deposits were irregular, and their crystalline grain tended to be finer. Both PASP and the modified PASPs (PASP-ASP, PASP-MEA and PASP-ASP-MEA) showed extremely good inhibition effects on $CaCO_3$ and $Ca_3(PO_4)_2$ scales. Particularly, PASP-ASP-MEA showed the smallest crystal scale deposits, and it had the best inhibition effects on $CaCO_3$ and $Ca_3(PO_4)_2$ scales. The synergy of the introduced hydroxyl and carboxylic groups of PASP-ASP-MEA can enhance the blocking

of the nano/microdust crystallization centers of $CaCO_3$ and $Ca_3(PO_4)_2$. Therefore, the rate of crystallization of $CaCO_3$ and $Ca_3(PO_4)_2$ decreased, which finally resulted in the smaller crystals [30–32].

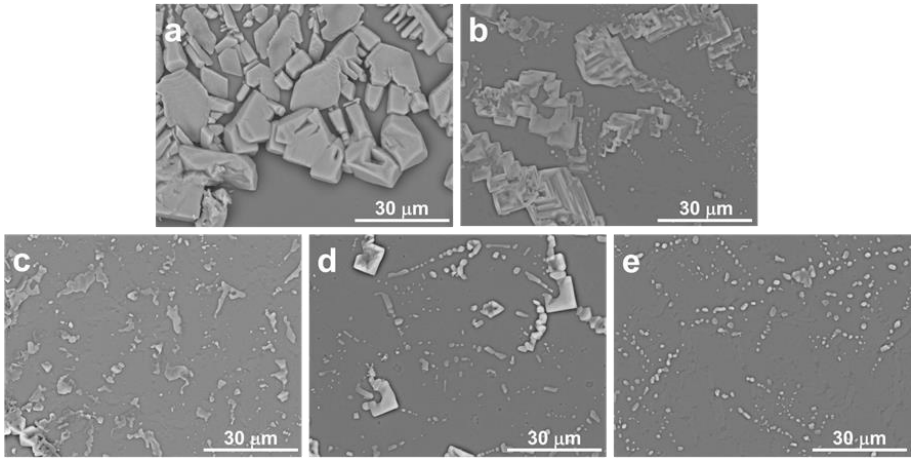

Figure 5. SEM images of $CaCO_3$ with PASP and its derivatives: (**a**) blank, (**b**) PASP, (**c**) PASP-ASP, (**d**) PASP-MEA, (**e**) PASP-ASP-MEA. (For PASP-ASP-MEA, the molar ratio of PSI–ASP–MEA was 1:0.5:0.5, reaction temperature was 0 °C, and reaction time was 24 h).

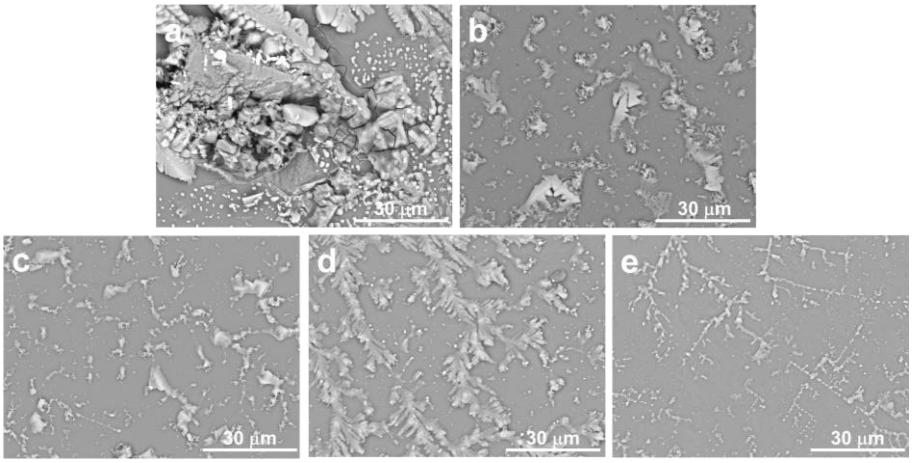

Figure 6. SEM images of $Ca_3(PO_4)_2$ with PASP and its derivatives: (**a**) blank, (**b**) PASP, (**c**) PASP-ASP, (**d**) PASP-MEA, (**e**) PASP-ASP-MEA. (For PASP-ASP-MEA, the molar ratio of PSI–ASP–MEA was 1:0.5:0.5, reaction temperature was 0 °C, and reaction time was 24 h).

XRD spectra of $CaCO_3$ crystals are shown in Figure 7. There are strong diffraction peaks of 26.2°, 27.2°, 33.1°, 36.2°, 37.3°, 45.9°, 50.2°, and 51.9° in Figure 7a, which are characteristic peaks of aragonite, and there are also diffraction peaks of 29.4° and 43.2° for calcite. These results indicate that in the absence of PASP and the modified PASPs, the calcium carbonate precipitate is the mixture of aragonite, which is the main crystal form, and some calcite [33]. In the other spectra (Figure 7b–e), diffraction peaks (24.9°, 27.1°, 32.8°, 43.9°, and 50.1°) corresponding to vaterite are very strong, which demonstrates that vaterite is the main crystal form in the presence of PASP and the modified PASPs [34]. Obviously, the vaterite peaks are the weakest for PASP-ASP-MEA. The change of crystal forms indicates that PASP-ASP-MEA contributed to the distortion of $CaCO_3$ crystals and showed the best inhibition effect on $CaCO_3$ scales.

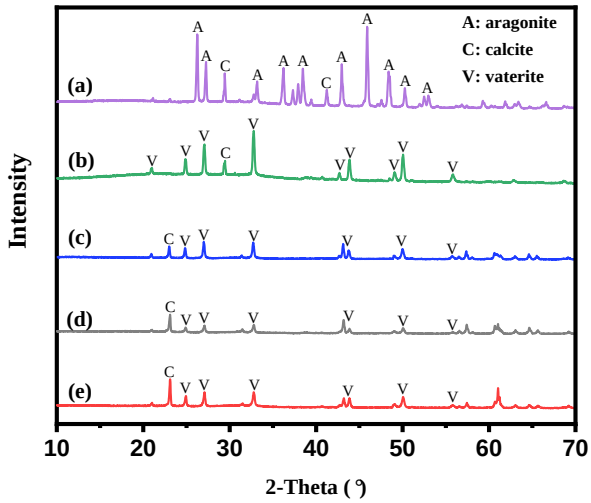

Figure 7. The XRD patterns of the $CaCO_3$ crystals: (a) blank, (b) PASP, (c) PASP-ASP, (d) PASP-MEA, (e) PASP-ASP-MEA. (For PASP-ASP-MEA, the molar ratio of PSI–ASP–MEA was 1:0.5:0.5, reaction temperature was 0 °C, and reaction time was 24 h).

The XRD spectra for $Ca_3(PO_4)_2$ crystals in the absence and in the presence of PASP and the modified PASPs (PASP-ASP, PASP-MEA and PASP-ASP-MEA) are shown in Figure 8. In spectrum a, there are strong diffraction peaks at the 22.9°, 29.3°, 36.0°, 39.3°, 43.0°, 47.4°, 48.3°, 57.5°, 60.6°, 64.6° and 65.5°, which are characteristic peaks of $Ca_3(PO_4)_2$ crystals [35], and the peak at 29.3° is obviously reduced in spectra b, c, d, and e. The addition of PASP and the modified PASPs (PASP-ASP, PASP- MEA, and PASP-ASP-MEA) showed a large influence on the crystal structure, and the diffraction peaks became quite weak after the addition of PASP and the modified PASPs, which implies that the surface morphology and particle size changed in the presence of the inhibitor. The diffraction peaks are the weakest for PASP-ASP-MEA, which shows that PASP-ASP-MEA had the best inhibition effect on $Ca_3(PO_4)_2$ scales.

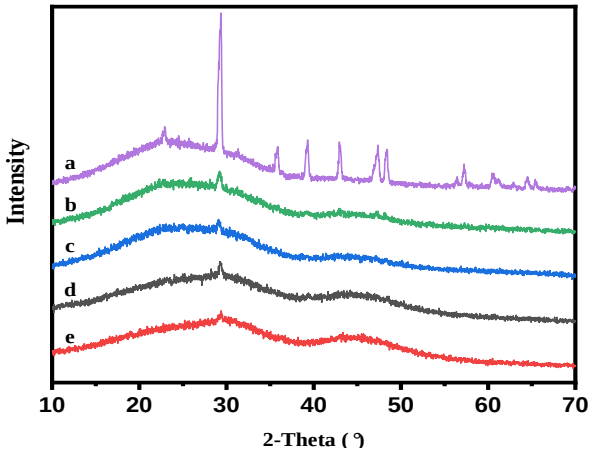

Figure 8. The XRD patterns of the $Ca_3(PO_4)_2$ crystals: (a) blank, (b) PASP, (c) PASP-ASP, (d) PASP-MEA, (e) PASP-ASP-MEA. (For PASP-ASP-MEA, the molar ratio of PSI–ASP–MEA was 1:0.5:0.5, reaction temperature was 0 °C, and reaction time was 24 h).

According to the above SEM images and XRD analysis, the introduction of the modified PASP disturbed the crystal growth habits and distorted the lattice, which resulted changes in the crystal morphology of the precipitates. The synergy of the introduced functional groups of PASP-ASP-MEA made the scale crystal become much smaller compared

with the effects of other inhibitors. Consequently, the scales become floppy and can be removed easily.

2.4. Biodegradation Performance of the Modified PASP

The biodegradation property of the modified PASP was investigated, and the results are shown in Figure 9. Compared with the pure PASP, the modified PASP showed a decreased biodegradation rate. This may be attributed to the formed cross-linked chemical bonds in the modified PASP [36,37]. However, it still experienced an easy degradation process; more than 60 and 70 wt% was lost after 21 and 28 days of biodegradation, respectively. When the polymers were catalyzed by the bacteria, the cross-linking chain and their backbone were both degraded and ruptured. They were first degraded to oligomers and smaller molecules and then biocatalyzed to carbon dioxide and water [38,39]. The modified PASP showed good biodegradable performance; it is indubitably an environmentally friendly scale inhibitor.

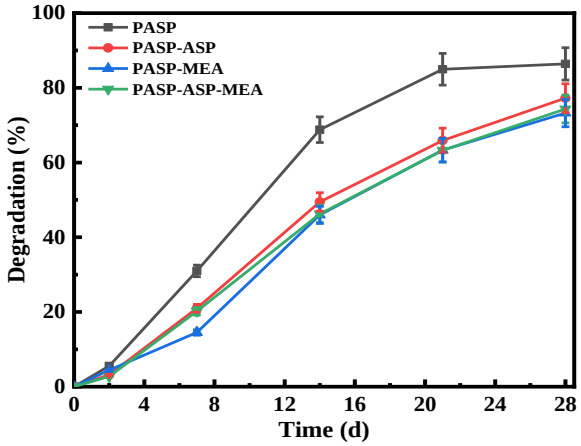

Figure 9. Degradation of PASP and the modified PASPs. (For PASP-ASP-MEA, the molar ratio of PSI–ASP–MEA was 1:0.5:0.5, reaction temperature was 0 °C, and reaction time was 24 h).

3. Experiment

3.1. Materials

L-aspartic acid was obtained from Changmao Biochemical Engineering Co., Ltd. (Changzhou, China). Ethanol, sodium hydrate, phosphoric acid, monoethanolamine (MEA), bromoethane, ethyl acetate, N,N-dimethylformamide (DMF), ethylene diamine tetraacetic acid (EDTA), calcium chloride, potassium dihydrogen phosphate, sodium bicarbonate, and sodium borate were purchased from Sinopharm Chemical Reagent Co., Ltd. (Shanghai, China) and were used as received without further purification. N-methylimidazole was supplied by Shanghai Aladdin Bio-Chem Technology Co., Ltd. (Shanghai, China). EmimH_2PO_4 was synthesized in our laboratory (Scheme 1) [40]. Deionized water (ultrafiltered to 18 MW×cm using a Milipore Milli-Q gradient system) was used in all experiments.

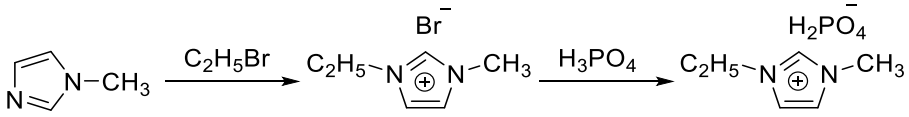

Scheme 1. Synthesis route of EmimH_2PO_4.

3.2. Characterization

Fourier transform infrared spectrometry (FTIR) was carried out on a Perkin-Elmer SpectrumGX Fourier transform infrared spectrometer (Waltham, MA, USA). Proton NMR

spectra were recorded on a Bruker Ascend 400 MHz nuclear magnetic resonance (NMR) spectrometer (Bruker, Billerica, MA, USA) using D_2O as solvent. Gel chromatography (GPC) (PL-GPC50, UK) was used to determine the molecular mass of polymers. Scanning electron microscopy (SEM, HITACHI TM3000, Tokyo, Japan) was used to capture the crystal structure of $CaCO_3$ and $Ca_3(PO_4)_2$. X-ray diffraction (XRD) was used to analyze the crystal form of $CaCO_3$ and $Ca_3(PO_4)_2$.

3.3. Synthesis of Polyaspartic Acid (PASP) in Ionic Liquid

L-aspartic acid (5 g) was dissolved in a three-necked flask. Ionic liquid 1-ethyl-3-methylimidazol dihydrogen phosphate ($EmimH_2PO_4$) (15 mL) was slowly added into the flask, and the mixture was reacted at 180 °C for 3 h. Afterwards, the mixture was poured into anhydrous ethanol to form the precipitate. Then, light yellow solid product was obtained. The product polysuccinimide (PSI) was filtrated and dry.

PSI (5 g) and 10 wt% hydroxide solution were added into a round bottom flask together. The mixture was stirred at 40 °C for 1 h. Then, the solution was filtered, washed with absolute alcohol, and dried. Finally, the reddish-brown product was obtained. The relevant synthetic reaction is expressed in Scheme 2.

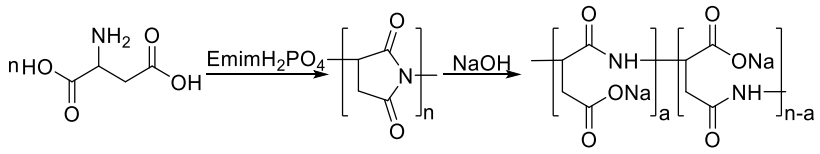

Scheme 2. Synthesis of PASP in ionic liquid.

3.4. Ring-Opening Graft Modification of PASP

PSI (2 g) and NH_3-NH_4Cl buffer solution (pH = 10, 20 mL) were mixed at 0 °C. Then, ASP (0.055 g, 0.044 g, 0.027 g, 0.011 g) and MEA (0.025 g, 0.020 g, 0.013 g, 0.005 g) were added to the mixture together. The reaction was carried out at 0 °C for 24 h under stirring. The reddish-brown viscous solid was obtained after the precipitate was washed with ethanol. The relevant synthetic reaction is expressed in Scheme 3. High performance liquid chromatography (HPLC) was used to detect the surplus amount of ASP, and gas chromatography (GC) was used to detect the surplus amount of MEA.

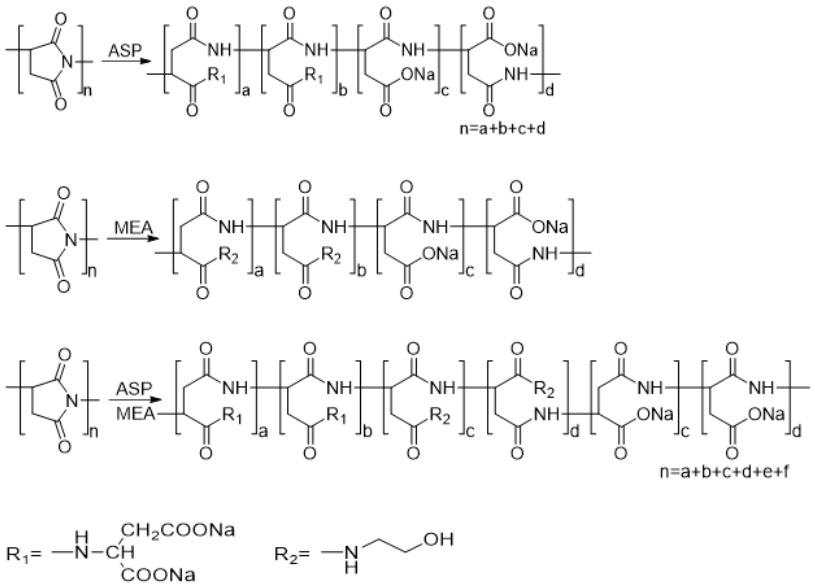

Scheme 3. Ring-opening graft modification of PASP.

The grafting ratio (GD, %) was calculated by the following Equation (1):

$$GD = \frac{m_1 - m_2}{m_1} \quad (1)$$

where m_1 is the feed amount of ASP or MEA and m_2 is the surplus amount of ASP or MEA.

3.5. Measurement of the Efficiency of Static Scale Inhibition

Static scale inhibition tests were performed according to Chinese National Standards GB/T 16632-2008 and GB/T 22626-2008. The experimental condition of scale inhibition to $CaCO_3$ was $CaCl_2$ (240 mg·L^{-1}) mixed with $NaHCO_3$ (732 mg·L^{-1}). The experimental condition of scale inhibition of $Ca_3(PO_4)_2$ was $CaCl_2$ (100 mg·L^{-1}) mixed with KH_2PO_4 (5 mg·L^{-1}). Borax buffer solution was used as the initial solution (pH = 9.0, 0.01 mol·L^{-1}). Both brines passed filtration (220 nm filter membrane) before use. The reaction was carried out at 80 °C for 10 h with various amounts of scale inhibitors. When the reaction was finished, it was cooled to room temperature and filtered by filter paper. The filtrate was titrated with ethylene diamine tetraacetic acid (EDTA) standard solution to determine the concentration of Ca^{2+} ($CaCO_3$).

The inhibition efficiency of $CaCO_3$ was calculated by the following Equation (2):

$$\eta_1 = \frac{\rho_2 - \rho_1}{\rho_0 - \rho_1} \times 100\% \quad (2)$$

where ρ_0 is the concentration of Ca^{2+} before experiment, ρ_1 is the concentration of Ca^{2+} in the absence of scale inhibitor in the solution, and ρ_2 is the concentration of Ca^{2+} in the presence of scale inhibitor in the solution.

The PO_4^{3-} concentration in the filtrate was detected by the ammonium molybdate spectrophotometric method. The inhibition efficiency of $Ca_3(PO_4)_2$ was calculated by the following Equation (3):

$$\eta_2 = \frac{\rho_2 - \rho_1}{\rho_0 - \rho_1} \times 100\% \quad (3)$$

where ρ_0 is the concentration of PO_4^{3-} before experiment, ρ_1 is the concentration of PO_4^{3-} in the absence of scale inhibitor, and ρ_2 is the concentration of PO_4^{3-} in the presence of inhibitor.

3.6. Biodegradation of the Modified PASP

The biodegradability of the modified PASP was estimated based on Chinese National Standard GB/T 21803-2008. The sample was treated with the standard activated sludge, which was obtained from Nanjing High Tech University Biological Technology Research Institute Co. Ltd., at 30 ± 1 °C for 28 days. The concentration of the activated sludge was 3~5 g/L. The concentration of the modified PASP was 100 mg/L. Sodium acetate was used as the standard molecule to estimate the activity of the standard activated sludge. The chemical oxygen demand (COD) detection was used to evaluate the biodegradability of the modified PASP. The COD was measured using a thermostat, DRB200 (Hach Co. Ltd., Loveland, CO, USA) and a spectrophotometer, DR1010 (Hach Co. Ltd., Loveland, CO, USA).

4. Conclusions

A new PASP-based green scale inhibitor (PASP-ASP-MEA) was obtained by ring-opening graft modification of PASP with both aspartic acid (ASP) and monoethanolamine (MEA). The modified PASP had excellent inhibition efficiency against $CaCO_3$ and $Ca_3(PO_4)_2$ scales. When the concentration of PASP-ASP-MEA was increased to 2 mg/L, its inhibition efficiency increased to 99% against $CaCO_3$ and 89% against $Ca_3(PO_4)_2$. Inhibition efficiency of 100% against both $CaCO_3$ and $Ca_3(PO_4)_2$ was achieved at a scale inhibitor dosage of 4 mg/L. The functional groups of PASP-ASP-MEA have good sorption on nano/microdust

surface. PASP-ASP-MEA can therefore block the nano/microdust crystallization centers of $CaCO_3$ and $Ca_3(PO_4)_2$ and significantly decrease the crystallization rate of these sparingly soluble salts. Compared with PASP-ASP and PASP-MEA, the synergy of the introduced groups (-OH and -CO_3) of PASP-ASP-MEA inevitably led better blocking of nano/microdusts. Thus, the scale crystals of $CaCO_3$ and $Ca_3(PO_4)_2$ became much smaller, increasing the solubility of these calcium salts in water. Moreover, the modified PASP also shows good biodegradable performance. In short, it is a promising green scale inhibitor.

Supplementary Materials: The following are available online at https://www.mdpi.com/article/10.3390/catal11070802/s1, Figure S1: Proton NMR spectra of PASP and PASP derivatives: (a) PASP, (b) PASP-ASP, (c) PASP-MEA, and (d) PASP-ASP-MEA. (For PASP-ASP-MEA, the molar ratio of PSI–ASP–MEA was 1:0.5:0.5, reaction temperature was 0 °C, and reaction time is 24 h).

Author Contributions: Formal Analysis, Y.Z.; Investigation, Y.Z. and Y.F.; Writing—Original Draft Preparation, Y.Z.; Writing—Review & Editing, J.W.; Supervision, Y.F.; Project Administration, Y.F.; Funding Acquisition, Y.F. Validation, Y.F. and Y.Z. All authors have read and agreed to the published version of the manuscript.

Funding: This research was funded by the National Natural Science Foundation of China, grant number 21805135; the Jiangsu Province Natural Science Foundation for Youths, grant number BK20180712 and the Postgraduate Research & Practice Innovation Program of Jiangsu Province (SJCX21_0546); The APC was funded by the National Natural Science Foundation of China and the Jiangsu Province Natural Science Foundation for Youths.

Acknowledgments: We are grateful for the technical discussions with Yuzhen Li for the measurement of the morphology of the Efficiency of Static Scale Inhibition, and Xiao Chen for the analysis of the biodegradation.

Conflicts of Interest: The authors declare no conflict of interest.

References

1. Antony, A.; Low, J.H.; Gray, S.; Childress, A.E.; Le-Clech, P.; Leslie, G. Scale formation and control in high pressure membrane water treatment systems: A review. *J. Membr. Sci.* **2011**, *383*, 1–16. [CrossRef]
2. Wolowiec, M.; Komorowska-Kaufman, M.; Pruss, A.; Rzepa, G.; Bajda, T. Removal of heavy metals and metalloids from water using drinking water treatment residuals as adsorbents: A review. *Minerals* **2019**, *9*, 17. [CrossRef]
3. Guo, Y.R.; Hu, Y.; Shi, K.; Bilan, Y. Valuation of water resource green efficiency based on SBM-TOBIT panel model: Case study from henan province, China. *Sustainability* **2020**, *12*, 6944. [CrossRef]
4. Zhang, S.P.; Qu, H.J.; Yang, Z.; Fu, C.E.; Tian, Z.Q.; Yang, W.B. Scale inhibition performance and mechanism of sulfamic/amino acids modified polyaspartic acid against calcium sulfate. *Desalination* **2017**, *419*, 152–159. [CrossRef]
5. Yu, W.; Song, D.; Chen, W.; Yang, H. Antiscalants in RO membrane scaling control. *Water Res.* **2020**, *183*, 115985. [CrossRef]
6. Yin, Y.M.; Jeong, N.; Minjarez, R.; Robbins, C.A.; Carlson, K.H.; Tong, T.Z. Contrasting behaviors between gypsum and silica scaling in the presence of antiscalants during membrane distillation. *Environ. Sci. Technol.* **2021**, *55*, 5335–5346. [CrossRef] [PubMed]
7. Feng, J.Y.; Gao, L.J.; Wen, R.Z.; Deng, Y.Y.; Wu, X.J.; Deng, S.L. Fluorescent polyaspartic acid with an enhanced inhibition performance against calcium phosphate. *Desalination* **2014**, *345*, 72–76. [CrossRef]
8. Chen, J.X.; Chen, F.J.; Han, J.; Su, M.; Li, Y.H. Evaluation of scale and corrosion inhibition of modified polyaspartic acid. *Chem. Eng. Technol.* **2020**, *43*, 1048–1058. [CrossRef]
9. Chen, Y.Y.; Zhou, Y.M.; Yao, Q.Z.; Nan, Q.L.; Zhang, M.J.; Sun, W. Synthesis of modified polyepoxysuccinic acid and evaluation of its scale inhibition on CaCO3, CaSO4, and Ca3(PO4)2 precipitation for industrial recycling water. *Desalin. Water Treat.* **2019**, *152*, 16–25. [CrossRef]
10. Hasson, D.; Shemer, H.; Sher, A. State of the art of friendly "green" scale control inhibitors: A review article. *Ind. Eng. Chem. Res.* **2011**, *50*, 7601–7607. [CrossRef]
11. Li, H.S.; Liu, W.; Qi, X.J. Evaluation of a novel CaSO4 scale inhibitor for a reverse osmosis system. *Desalination* **2007**, *214*, 193–199. [CrossRef]
12. Zhu, T.Z.; Wang, L.D.; Sun, W.; Yang, Z.Q.; Wang, S.L.; Zhao, L.Q.; Xiao, G.J.; Wang, G.Z.; Liu, Z.M.; Shu, X.Q.; et al. Local scaling of CaCO3 on carbon steel surface with different corrosion types. *Powder Technol.* **2019**, *356*, 990–1000. [CrossRef]
13. Mady, M.F.; Bayat, P.; Kelland, M.A. Environmentally friendly phosphonated polyetheramine scale inhibitors-excellent calcium compatibility for oilfield applications. *Ind. Eng. Chem. Res.* **2020**, *59*, 9808–9818. [CrossRef]
14. Can, H.K.; Uner, G. Water-soluble anhydride containing alternating copolymers as scale inhibitors. *Desalination* **2015**, *355*, 225–232. [CrossRef]

15. Martinod, A.; Neville, A.; Euvrad, M.; Sorbie, K. Electrodeposition of a calcareous layer: Effects of green inhibitors. *Chem. Eng. Sci.* **2009**, *64*, 2413–2421. [CrossRef]
16. Mazumder, M.A.J. A review of green scale inhibitors: Process, types, mechanism and properties. *Coatings* **2020**, *10*, 928. [CrossRef]
17. Zhang, Z.J.; Lu, M.L.; Liu, J.; Chen, H.L.; Chen, Q.L.; Wang, B. Fluorescent-tagged hyper-branched polyester for inhibition of CaSO4 scale and the scale inhibition mechanism. *Mater. Today Commun.* **2020**, *25*, 101359. [CrossRef]
18. Migahed, M.A.; Rashwan, S.M.; Kamel, M.M.; Habib, R.E. Synthesis, characterization of polyaspartic acid-glycine adduct and evaluation of their performance as scale and corrosion inhibitor in desalination water plants. *J. Mol. Liq.* **2016**, *224*, 849–858. [CrossRef]
19. Ketrane, R.; Saidani, B.; Gil, O.; Leleyter, L.; Baraud, F. Efficiency of five scale inhibitors on calcium carbonate precipitation from hard water: Effect of temperature and concentration. *Desalination* **2009**, *249*, 1397–1404. [CrossRef]
20. Ling, L.; Zhou, Y.M.; Huang, J.Y.; Yao, Q.Z.; Liu, G.Q.; Zhang, P.X.; Sun, W.; Wu, W.D. Carboxylate-terminated double-hydrophilic block copolymer as an effective and environmental inhibitor in cooling water systems. *Desalination* **2012**, *304*, 33–40. [CrossRef]
21. Nudelman, F.; Pieterse, K.; George, A.; Bomans, P.H.H.; Friedrich, H.; Brylka, L.J.; Hilbers, P.A.J.; de With, G.; Sommerdijk, N. The role of collagen in bone apatite formation in the presence of hydroxyapatite nucleation inhibitors. *Nat. Mater.* **2010**, *9*, 1004–1009. [CrossRef] [PubMed]
22. Nemethy, A.; Solti, K.; Kiss, L.; Gyarmati, B.; Deli, M.A.; Csanyi, E.; Szilagyi, A. pH- and temperature-responsive poly(aspartic acid)-l-poly (N-isopropylacrylamide) conetwork hydrogel. *Eur. Polym. J.* **2013**, *49*, 2392–2403. [CrossRef]
23. Xu, Y.; Wang, L.N.; Zhao, L.L.; Cui, Y.C. Synthesis of polyaspartic acid-aminobenzenesulfonic acid grafted copolymer and its scale inhibition performance and dispersion capacity. *Water Sci. Technol.* **2011**, *64*, 423–430. [CrossRef]
24. Zhang, Q.; Vigier, K.D.O.; Royer, S.; Jérôme, F. Deep eutectic solvents: Syntheses, properties and applications. *Chem. Soc. Rev.* **2012**, *41*, 7108–7146. [CrossRef]
25. Wang, B.S.; Qin, L.; Mu, T.C.; Xue, Z.M.; Gao, G.H. Are ionic liquids chemically stable? *Chem. Rev.* **2017**, *117*, 7113–7131. [CrossRef]
26. Reddy, P.N.; Padmaja, P.; Reddy, B.V.S.; Rambabu, G. Ionic liquid/water mixture promoted organic transformations. *RSC Adv.* **2015**, *5*, 51035–51054. [CrossRef]
27. Coxon, J.M.; Townsend, M.A.E. Computational study on the ring-opening reaction of protonated oxirane and methylpropene. *Tetrahedron* **2007**, *63*, 5665–5668. [CrossRef]
28. Quan, Z.H.; Chen, Y.C.; Wang, X.R.; Shi, C.; Liu, Y.J.; Ma, C.F. Experimental study on scale inhibition performance of a green scale inhibitor polyaspartic acid. *Sci. China Ser. B Chem.* **2008**, *51*, 695–699. [CrossRef]
29. Tang, Y.M.; Yang, W.Z.; Yin, X.S.; Liu, Y.; Yin, P.W.; Wang, J.T. Investigation of CaCO3 scale inhibition by PAA, ATMP and PAPEMP. *Desalination* **2008**, *228*, 55–60. [CrossRef]
30. Oshchepkov, M.; Golovesov, V.; Ryabova, A.; Frolova, S.; Tkachenko, S.; Kamagurov, S.; Rudakova, G.; Popov, K. Synthesis and visualization of a novel fluorescent-taggedpolymeric antiscalant during gypsum crystallization in combination with bisphosphonate fluorophore. *Crystals* **2020**, *10*, 992. [CrossRef]
31. Oshchepkov, M.; Golovesov, V.; Ryabova, A.; Tkachenko, S.; Redchuk, A.; Ronkkomaki, H.; Rudakova, G.; Pervov, A.; Popov, K. Visualization of a novel fluorescent-tagged bisphosphonate behavior during reverse osmosis desalination of water with high sulfate content. *Sep. Purif. Technol.* **2021**, *255*, 117382. [CrossRef]
32. Chai, C.X.; Xu, Y.H.; Li, D.Y.; Zhao, X.W.; Xu, Y.; Zhang, L.; Wu, Y.F. Cysteamine modified polyaspartic acid as a new class of green corrosion inhibitor for mild steel in sulfuric acid medium: Synthesis, electrochemical, surface study and theoretical calculation. *Prog. Org. Coat.* **2019**, *129*, 159–170. [CrossRef]
33. Liu, D.; Dong, W.B.; Li, F.T.; Hui, F.; Ledion, J. Comparative performance of polyepoxysuccinic acid and polyaspartic acid on scaling inhibition by static and rapid controlled precipitation methods. *Desalination* **2012**, *304*, 1–10. [CrossRef]
34. Wang, H.C.; Zhou, Y.M.; Yao, Q.Z.; Ma, S.S.; Wu, W.D.; Sun, W. Synthesis of fluorescent-tagged scale inhibitor and evaluation of its calcium carbonate precipitation performance. *Desalination* **2014**, *340*, 1–10. [CrossRef]
35. Naciri, Y.; Hsini, A.; Ajmal, Z.; Bouddouch, A.; Bakiz, B.; Navio, J.A.; Albourine, A.; Valmalette, J.C.; Ezahri, M.; Benlhachemi, A. Influence of Sr-doping on structural, optical and photocatalytic properties of synthesized Ca3(PO4)2. *J. Colloid Interface Sci.* **2020**, *572*, 269–280. [CrossRef] [PubMed]
36. Nakato, T.; Tomida, M.; Suwa, M.; Morishima, Y.; Kusuno, A.; Kakuchi, T. Preparation and characterization of dodecylamine-modified poly(aspartic acid) as a biodegradable water-soluble polymeric material. *Polym. Bull.* **2000**, *44*, 385–391. [CrossRef]
37. Juriga, D.; Nagy, K.; Jedlovszky-Hajdu, A.; Perczel-Kovach, K.; Chen, Y.M.; Varga, G.; Zrinyi, M. Biodegradation and osteosarcoma cell cultivation on poly(aspartic acid) based hydrogels. *ACS Appl. Mater. Interfaces* **2016**, *8*, 23463–23476. [CrossRef] [PubMed]
38. Huang, K.; Kong, L. Preparation and characterization of poly(aspartic acid) derivatives as biodegradable water treatment agents. *Asian J. Chem.* **2013**, *25*, 10233–10237. [CrossRef]
39. Yang, J.H.; Liu, T.; Liu, H.B.; Zhang, D.; Zhai, L.M.; Liu, J.; Wang, M.; Chen, Y.X.; Chen, B.Y.; Wang, H.Y. Biodegradable PASP can effectively inhibit nitrification, moderate NH3 emission, and promote crop yield. *Arch. Agron. Soil Sci.* **2019**, *65*, 1273–1286. [CrossRef]
40. Dong, F.; Jun, L.; Zhou, X.L.; Liu, Z.L. Mannich reaction in water using acidic ionic liquid as recoverable and reusable catalyst. *Catal. Lett.* **2007**, *116*, 76–80. [CrossRef]